# Three Dimensional CFD Simulation on Two Row Plane Fin Heat Exchanger

**Brijesh Kumar Sen[1] Prof. Amit Khare[2] Prof. Shamir Daniel[3]**
[1,2,3]TIEIT College, Karond Gandhi Nagar, Bypass Road, Bhopal MP, India

*Abstract*— Three-dimensional CFD simulations are carried out to investigate heat transfer and fluid flow characteristics of a two-row plain fin-and-tube heat exchanger using ANSYS FLUENT. Heat transfer and pressure drop characteristics of the heat exchanger are investigated for Reynolds numbers ranging from 330 to 7200. Model geometry is created, meshed, calculated, and post-processed using ANSYS Workbench. Fluid flow and heat transfer are simulated and results compared using both laminar and turbulent flow models (k-epsilon, and SST k-omega), with steady-state solvers to calculate pressure drop, flow, and temperature fields. Model validation is carried out by comparing the simulated case friction factor f and Colburn j factor with experimental results from the literature. For friction factor determination, little difference is found between the flow models simulating laminar flow, while in transitional flow, the laminar flow model produced the most accurate results and the k-omega SST turbulence model was more accurate in turbulent flow regimes. The results of simulations for heat transfer in laminar flow using the laminar flow model are found to be in good agreement with the experimental results, while heat transfer in transitional flow is best represented with the SST k-omega turbulence model, and heat transfer in turbulent flow is more accurately simulated with the k-epsilon turbulence model. Reasonable agreement is found between the simulations and experimental data, and the ANSYS FLUENT software has been sufficient for simulating the flow fields in tube-fin heat exchangers.

***Keywords:*** Plate Heat Exchangers, Fin and Tube Exchanger, CFD, Reynold Number, Fanning Friction Factor F, Colburn J-Factor

## I. INTRODUCTION

Fin-and-tube heat exchangers are widely-used heat transfer devices in applications like refrigeration and air conditioning systems. It's easier manufacturing, simpler construction, lower cost, and relatively easy in maintenance makes it one of the most commonly used heat exchangers. A heat exchanger is a system used to transfer heat between two or more fluids. Heat exchangers are used in both cooling and heating processes. The fluids may be separated by a solid wall to prevent mixing or they may be in direct contact. They are widely used in space heating, refrigeration, air conditioning, power stations, chemical plants, petrochemical plants, petroleum refineries, natural-gas processing, and sewage treatment.

### *A. Plate fin heat exchanger*

This type of heat exchanger uses "sandwiched" passages containing fins to increase the effectiveness of the unit. The designs include cross flow and counter flow coupled with various fin configurations such as straight fins, offset fins and wavy fins.

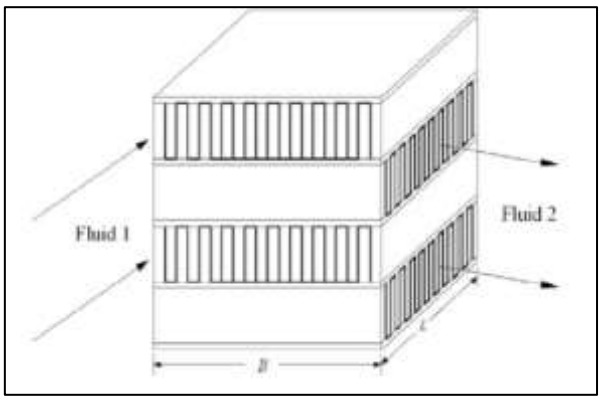


Fig. 1.5: Plate Fin Heat Exchanger

Plate and fin heat exchangers are usually made of aluminium alloys, which provide high heat transfer efficiency. The material enables the system to operate at a lower temperature difference and reduce the weight of the equipment. Plate and fin heat exchangers are mostly used for low temperature services such as natural gas, helium and oxygen liquefaction plants, air separation plants and transport industries such as motor and aircraft engines.

### *B. Finned Tube Heat Exchanger*

The usage of fins in a tube-based heat exchanger is common when one of the working fluids is a low-pressure gas, and is typical for heat exchangers that operate using ambient air, such as automotive radiators and HVAC air condensers. Fins dramatically increase the surface area with which heat can be exchanged, which improves the efficiency of conducting heat to a fluid with very low thermal conductivity, such as air. The fins are typically made from aluminium or copper since they must conduct heat from the tube along the length of the fins, which are usually very thin.

Fig. 1.6: Finned Tube Heat Exchanger

### *C. Objectives of the Research*

The present study is carried out on triangular shaped secondary fins, with delta/rectangular wings on their slant faces, sandwiched between the parallel plates of plate-fin heat exchanger.

- To visualize the cross-stream velocity vectors along and beyond the wing vortex generator. Secondary flow structure is analyzed as the fluid passes over the vortex generator.
- To simulate the vorticity contours to get the idea of the strength of the crossstream velocity vectors.

 

- To determine the heat transfer characteristics in terms of combined spanwise average Nusselt number and the bulk temperature. Nusselt number is a measure of the efficiency of heat transfer and the bulk temperature is a direct measure of thermal energy.
- To compute the reduction in the length of heat exchanger for a particular bulk temperature at the exit of the exchanger. To study the effect of varying the Reynolds number on the heat transfer enhancement and the pressure drop for delta and rectangular wings.
- To study the effect of varying the Reynolds number on the heat transfer enhancement and the pressure drop for delta and rectangular wings.
- To simulate the effect of stamped-wing vortex generator and compare it with the results pertaining to built-in wing.
- To compare rectangular and delta wings for the same span and chord length and also for the same area of both the wings.

## II. PROBLEM FORMULATION

For this project, the geometrical parameters of a two-row heat exchanger based on experimental research [Wang et al., 1996] are used to build a CFD model, and results read from the graphs (friction factor and Colburn j-factor against Reynolds number) in the article are used to validate the results of the CFD simulations. The parameters of interest: friction factor f and Colburn j-factor are widely used in industry to characterize pressure drop and heat transfer, respectively, and thereby determine heat exchanger performance and suitability for specific duties. Determining and using these parameters for performance prediction is part of the heat exchanger design process.

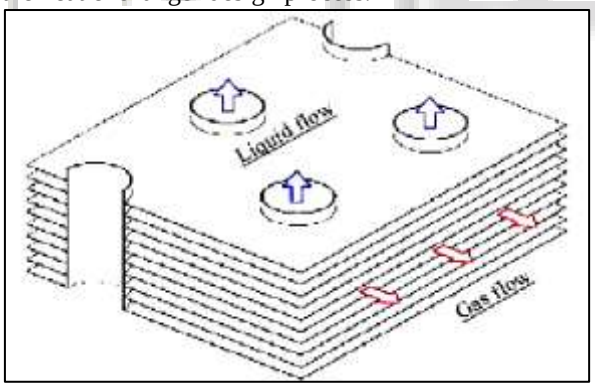


Fig. 1.10: Typical fin-and-tube heat exchanger section with staggered tube arrangement

The two-row fin-and-tube heat exchanger studied has a staggered tube arrangement. Analyzing flow and heat transfer using CFD can make calculations to predict heat exchanger performance easy. However, it is not possible to perform CFD simulation on the entire heat exchanger, due to the large number of volumes and calculations required. Therefore, a small section of a heat exchanger consisting of one channel of air between two fins, with the air flowing by two tubes is modeled for this project.

## III. MODEL DESCRIPTION

When fluids, surfaces, or combinations of these are at different temperatures and in thermal contact, heat exchangers are used to transfer thermal energy. Heat recovery, pasteurisation, distillation, and the heating or cooling of a specific fluid stream are examples of typical applications. A wall might divide the fluids or they can be in close touch. Appendages, or fins, can be connected to a wall acting as a heat transfer surface separating fluids in order to improve the heat transfer surface area.

Classification of Heat Exchangers

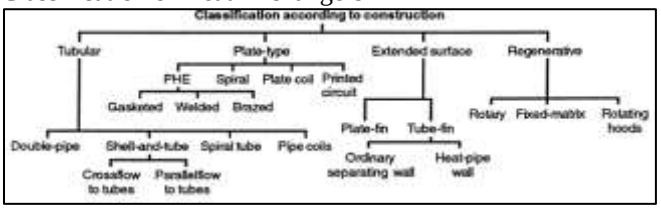


Fig. 3.1: Classification of Heat Exchangers

### A. Computational Domain

The pre-processing software ANSYS Design Modeler and Mesh module is used to create and mesh the computational model. A diagram of the studied model is shown in Figure 3.2, and consists of the air flow area between two fins of plain fin geometry and around the surfaces of two rows of tubes.

| Geometric Parameter | Symbol | Dimensions |
|---|---|---|
| Fin Thickness | t | 0.130 mm |
| Fin Pitch | Fp | 2.240 mm |
| Fin collar Outside Diameter | Dc | 10.23 mm |
| Transverse Pitch | Pt | 25.40 mm |
| Longitudinal Pitch | Pl | 22.00 mm |
| Tube Wall Thickness | δ | 0.336 mm |
| Number of Tube Rows | | 2 |

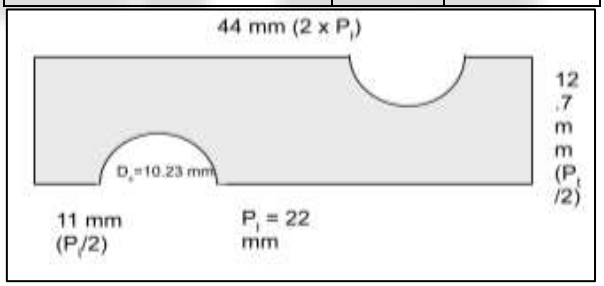


Fig. 3.2: The primary computational domain and geometric parameters of the heat exchanger

The computational domain is specified by 0 x 8Pl, 0 y Pt/2, and 0 z Fp, and is 8 times the original heat transfer area (as shown in Figure 3.2), while the actual modelled heat exchanger length is equal to twice the longitudinal pitch Pl. To decrease oscillations and assure a representative flow in the computational domain of the actual heat exchanger, the volume representing the air that travels through the gap between the two fins is enlarged upstream from the inlet and downstream from the outlet.

### *B. Boundary Condition*

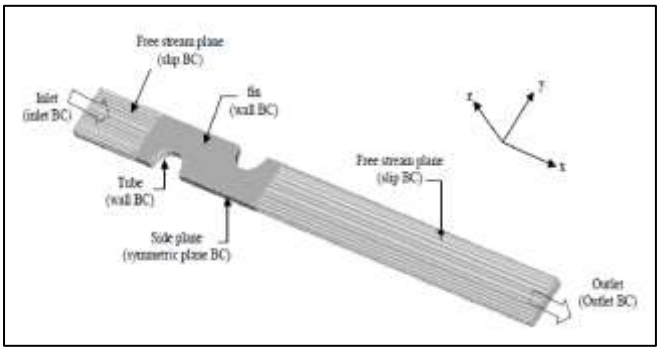


Fig. 3.3: Boundary conditions (BC) and extended flow volumes are included in the computational domain

Boundary conditions are present in the computational domain, as shown in Figure 3.3, with the following conditions:

Tube surfaces, Dirichlet BC:

$T = T_w$,

Air velocity: $u = v = w = 0$

Inlet, Dirichlet BC:

Uniform velocity $u = u_{in}$,

$v = w = 0$

$T = 5\ ^oC$.

Outlet, Neumann BC:

Zero gradients, u, v, w, pressure, and temperature. (One-way),

Free stream planes: (top and bottom planes of the extended surface areas):

'Slip' conditions: $(\partial u/\partial z) = 0$, $(\partial v/\partial z) = 0$, $w = 0$, $(\partial T/\partial z) = 0$.

Side planes: symmetry planes

$(\partial u/\partial y) = 0$, $v = 0$, $(\partial w/\partial y) = 0$, $(\partial T/\partial y) = 0$

The total computational domain was made up of 150521 finite volumes, with a structured grid running across most of it and an unstructured grid around the tubes. Based on the results of a grid independence test, the cell number was decided.

### *C. Governing Equations and Numerical Schemes*

The three-dimensional continuity, Navier-Stokes for momentum and energy, and scalar transport equations for steady-state flow are the governing equations for this project, and they can be stated (usually) as follows:

Equation of Continuity:

$$\frac{\partial(\rho u_i)}{\partial x_i} = 0. \tag{1}$$

Momentum equation:

$$\frac{\partial}{\partial x_i}(\rho u_i u_j) = \frac{\partial}{\partial x_i}\left(\mu \frac{\partial u_j}{\partial x_i}\right) - \frac{\partial p}{\partial x_j}. \tag{2}$$

Energy Equation:

$$\frac{\partial}{\partial x_i}(\rho u_i T) = \frac{\partial}{\partial x_i}\left(\frac{k}{C_p}\frac{\partial u_j}{\partial x_i}\right). \tag{3}$$

General Transport Equations (for scalers):

$$\frac{\partial(\rho u_i \phi)}{\partial x_i} = \frac{\partial}{\partial x_i}\left[\Gamma_\phi \frac{\partial \phi}{\partial x_i}\right] + S_\phi \tag{4}$$

In CFD calculations, the general equations 1-3 are used to determine the flow field for both thermal and fluid (air) dynamics, including heat transfer and pressure drop. The finite volume approach is used to discretize and solve them. It's solved on a staggered grid with laminar and turbulent flow solvers, with the latter using the Reynolds Averaged Navier-Stokes equations (RANS) with both k-epsilon and SST k-omega turbulence models. The SIMPLE algorithm is used to assure velocity and pressure coupling.

## IV. COMPUTED FLUID DYNAMICS

CFD (computational fluid dynamics) is a computer-based modelling tool for studying fluid flow, heat transfer, and related phenomena including combustion and chemical reactions. CFD is used in this project to analyse flow and heat transfer. Aerodynamic lift and drag (i.e. aeroplane or windmill wings), power plant combustion, chemical processes, heating/ventilation, and even biomedical engineering are some examples of application domains (simulating blood flow through arteries and veins). CFD analysis is utilised in the R&D and manufacturing of aeroplanes, combustion engines, and a variety of other industrial goods in many industries.

Since experiments have a cost directly proportionate to the number of configurations requested for testing, CFD can be advantageous over traditional experimental-based analysis because enormous amounts of results can be provided at virtually no additional cost. When compared to tests, parametric analyses to optimise equipment are quite inexpensive with CFD.

### *A. CFD Computational Tools*

This section explains the CFD tools needed to run a simulation as well as the steps involved in utilising CFD to address an issue. The hardware requirements as well as the three primary aspects of CFD simulation processing: the pre-processor, processor, and post-processor are discussed. Depending on the complexity of the mesh and the scale of the computations, commercial CFD software like as ANSYS Fluent, ANSYS CFX, and ACE are available, as well as a wide range of compatible hardware and associated expenses. Three major components are required to perform a simulation:

1) Pre-processor: To establish the geometry for the computational region of interest and generate the mesh of control volumes, a pre-processor is used (for calculations). In general, the finer the mesh in large-change areas, the more accurate the solution. The grid's fineness also influences the computer hardware and calculation time required. As a pre-processor, ANSYS Workbench's Design Modeler and Mesh tool are employed.
2) Solver: The solver uses a numerical solution methodology such as finite difference, finite element, or spectral approaches to perform the calculations. Finite volumes, a type of finite difference approach, are used in most CFD codes. The fluid flow equations are first integrated over the control volumes (resulting in accurate conservation of relevant properties for each finite volume), then discretized (creating algebraic equations by converting the integral fluid flow equations), and lastly solved using an iterative method.

 

3) Post-Processor: The results are visualised using the post-processor, which includes the ability to display geometry/mesh, produce vector, contour, and 2D and 3D surface plots. Particles may be monitored throughout a simulation, and the model can be altered (e.g., by scaling, rotating, and so on), all while seeing the simulation in full colour animated graphics. The post-processor utilised in this project is CFD Post.

*B. Problem-Solving with CFD*

There are many decisions to be made before setting up the problem in the CFD code. Some of the decisions to be made can include: whether the problem should be 2D or 3D, which type of boundary conditions to use, whether or not to calculate pressure/temperature variations based on the air flow density, which turbulence model to use etc. The assumptions made should be reduced to a level as simple as possible, yet still retaining the most important features of the problem to be solved in order to reach an accurate solution. Details of the heat exchanger geometry, initial boundary conditions related to flow and temperature were followed as closely as possible when building this CFD model.

*C. Solution Algorithm*

The SIMPLE algorithm is a guess-and-correct method for calculating pressure values on a staggered grid. When other scalars are calculated, it is iterative and must be done in a specified order. The technique's overall approach is depicted in the diagram below, which is followed by a description of the algorithm's steps.

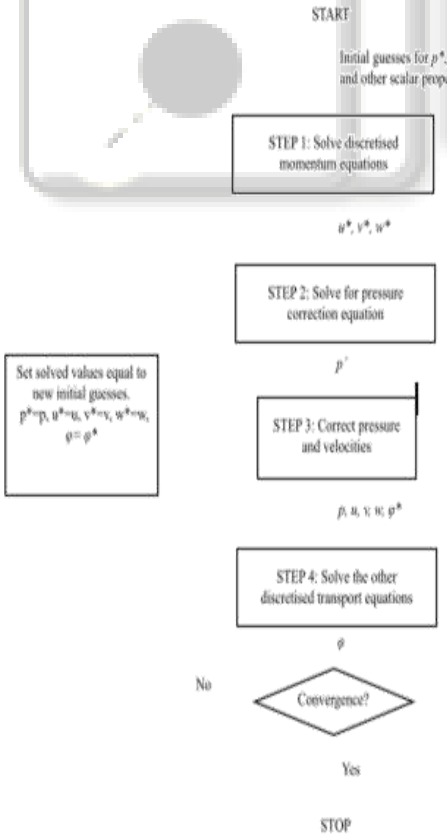


Fig. 4.2: Simple Algorithm

Steps of Simple Algorithm are summarized below:
START
Estimate a starting guess for the pressure field p*.
Step 1
Based on the pressure guess p*, solve the discretized momentum equations for the velocity components. Six discretised momentum balances are solved for each of the six neighbours for node P in a three-dimensional situation like the one in this project (W, E, S, N, B, and T). Based on p*, this phase finds values for u*, v*, and w*.
Step 2
To determine the pressure correction p', solve for the pressure correction equation. The discretised continuity equation is used to find the mass imbalance and the difference between total mass flow input and total mass flow outflow of the six 'guessed' velocities (derived using the guessed pressure p*).
Step 3
Reduce the measured pressure components using the pressure correction, in which the correction (p') is added to the initial guess (p*) to get the new pressure field p, or:

$$p = p^* + p'$$

This stage of the SIMPLE algorithm yields estimated values for velocity components and pressure: p, u, v, w, *, which fulfil the continuity equation.
Step 4
To calculate values for the remaining scalar variables φ, solve the remaining discretised transport equations using the line-TDMA approach.

*D. Convergence*

After step 4, the outputs are checked for convergence (meaning the mass imbalance is extremely close to zero), and if it isn't within the required range, the computer loops back to step 1, using the freshly calculated pressure, velocity, and other scalar values as the next starting guess. The process will continue until convergence is achieved (iteration).

*E. Relaxation Factors*

The pressure correction is frequently set too high, resulting in unstable calculations and divergence rather than convergence. The iteration technique must be slowed as a result of this issue in order to under-relax the pressure corrections. This is accomplished by multiplying the correction factor by an under-relaxation factor of 0 to 1, such that only a fraction of the initially calculated correction factor is used in the computation (for example, using the pressure correction):

$$p = p^* + \alpha_p p' \tag{25}$$

For the velocity components, under-relaxation factors are also used. Too large values for result in oscillatory or divergent solutions, while too small values for the under-relaxation factor result in extremely slow convergence. As a result, the correct under-relaxation factor is critical for a converged solution, but it is impossible to determine in general and must be determined for each individual CFD case.

 

## V. RESULTS AND DISCUSSION

### *A. Grid Independence Test*

The grid independence test is performed to see how the size of the grid impacts simulation results. The same geometric model is simulated with different grid sizes in this test. As an independent grid, we employ a mesh that has no effect on the simulation output. This is to reduce the inaccuracy caused by the grid size (discretisation error). For this project, pressure loss between inlet and outlet is simulated using 5 mesh sizes with 1360, 32850, 44199, 150521, and 275324 cells. Based on the comparison of simulated results, the grid of 150521 cells is chosen as the independent grid size for the project. Despite the fact that mesh sizes with 150521 and 275324 cells produce virtually identical results, the one with 150521 cells takes less time to compute.

### *B. Experimental Results*

#### *1) Experimental Values for Colburn j-Factor*

The Colburn j-factor decreases with increasing Reynolds number, as shown in Table 5.1 and Figure 5.1. The Reynolds number ranges from 0.042 at the lowest to 0.0081 at the highest. This graph for air flow through a heat exchanger has a more distinct dip in the transition region than a plot of this sort (j vs. Re) for a standard circular tube. However, at Reynolds number 1300, the graph appears to level off, and at Reynolds number 2900, the graph looks to level off again. As a result of this graph, it can be deduced that the laminar flow region extends up to roughly Reynolds number 1300 (precise values are impossible to determine without more data points), there is a transition phase after that, and turbulent flow begins at around Reynolds number 2900. These experimental data are compared to values for the Colburn j-factor derived from simulations and followed by the required calculations for this project. The uncertainties in the Colburn j-factor values (experimentally derived values) can be considerable at the lower Reynolds numbers (uncertainty is 9.4% at Reynolds number 600, and may be much higher at Reynolds number 330, the value of which was not mentioned in the text).

| Re | Colburn j factor |
|---|---|
| 330 | 0.042 |
| 600 | 0.027 |
| 790 | 0.023 |
| 1300 | 0.017 |
| 1700 | 0.014 |
| 2900 | 0.012 |
| 4300 | 0.0094 |
| 5200 | 0.009 |
| 6200 | 0.0084 |
| 7200 | 0.0081 |

Experimental values for Colburn j- factor

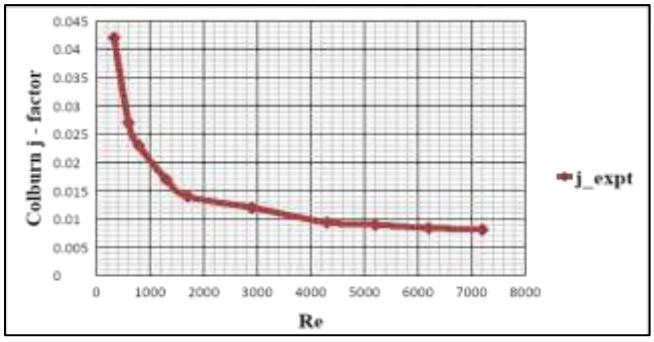


Plot of Reynolds Number Vs Colburn j- factor, determined experimentally

#### *2) Experimental Values for Fanning Friction Factor f*

The values for Reynolds number and friction factor f as read from the graph in the article for the specific heat exchanger shape explored in this project.

| Re | Friction factor f |
|---|---|
| 330 | 0.11 |
| 600 | 0.073 |
| 790 | 0.063 |
| 1300 | 0.046 |
| 1700 | 0.042 |
| 2900 | 0.033 |
| 4300 | 0.027 |
| 5200 | 0.024 |
| 6200 | 0.022 |
| 7200 | 0.021 |

Table 5.2: Experimental values for Fanning friction factor f

The Colburn j-factor, the Fanning friction factor f also decreases as the Reynolds number increases. It ranges from 0.11 at the lowest Reynolds number to 0.021 at the high Reynolds number. A slight change can be seen at Between Reynolds numbers 1300 and 1700, the graph levels off again. The laminar flow region appears to begin about Reynolds number 1300, with a transition region following, and the turbulent flow regime appears to begin at roughly Reynolds number 1700, based on the tiny change in the graph (or possibly it is closer to 2900 since that is what was found on the j-factor graph). More data points, on the other hand, would be required to precisely identify the critical Reynolds values for the various flow regimes. The uncertainties in the Fanning friction factor f values (experimentally determined values) can be large at the lower Reynolds numbers (the uncertainty is given as 17.7% at Reynolds number 600, and may be much higher for Reynolds number 330, the value of which was not provided in the text).

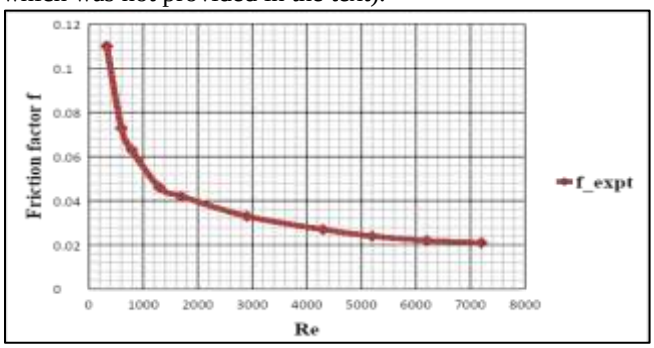


Fig. 5.2: Plot of Reynolds Number Vs Fanning friction factor f, determined experimentally

*C. Numerical Results*

*1) Characteristics of Flow*

After conducting the CFD simulations in ANSY Fluent, this part describes the observations made with CFD Post. With contour plots of velocity with vectors, the features of low-Reynolds flow and high-Reynolds flow are contrasted.

*2) Observations of Velocity*

The flow patterns of the two examples (inlet air velocity 0.3 m/s vs. 6.2 m/s) are comparable at low and high Reynolds numbers. The air enters from the left-hand inlet, flows in the direction of the arrows, and escapes out the right-hand outlet.

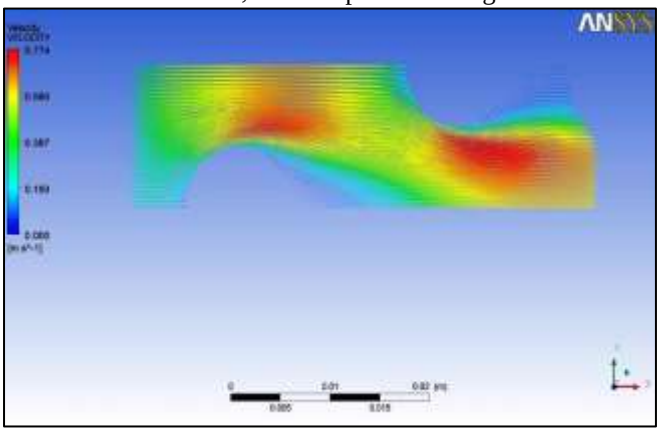

Velocity vector for inlet velocity 0.3 m/s, SST k-omega flow model

The air speeds up as it goes through the first tube in both cases, then speeds up again as it passes through the second tube. As indicated by the samples taken in the case files for average velocities at the minimal free-flow zones, the velocity flowing around the second tube is faster than the velocity flowing around the first tube. The minimum free-flow area is the area of the heat exchanger between two transverse tubes, so the area directly above tube one or just below tube two is the minimum free-flow area. In the air flow channel, the tubes work as a type of pipe constriction, forcing the flow to accelerate.

The areas with the highest velocity are just off the streamlines that travel directly around the tubes, and are in the least free-flowing area. In the instance of a 0.3 m/s inlet velocity, the top velocity at the second tube is 0.77 m/s, or roughly 2.5 times the inlet velocity. For the 6.2 m/s inlet flow example, the greatest velocity is 14.55 m/s, which is more than twice the intake velocity.

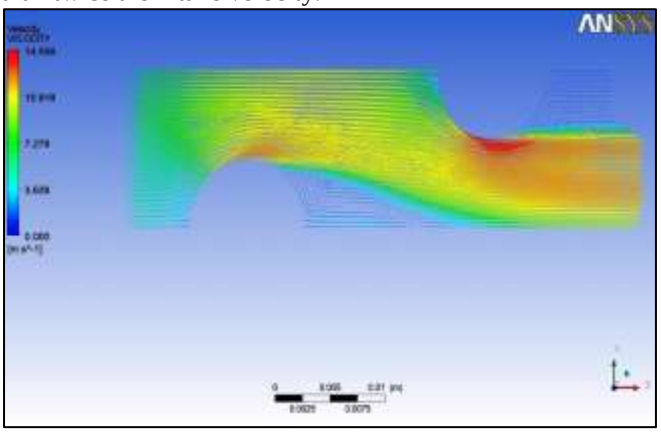

Fig. 5.4: Velocity vector for inlet velocity 6.2 m/s, SST k-omega flow model

The size of the tubes has an effect on the Reynolds number of the air flowing around them, because with larger tubes (at the same distance from each other), the minimum free-flow area would be even smaller if the transverse pitch stayed the same. The tube collar diameter is used as the characteristic length for the Reynolds number in this study, and it can be observed that increasing this parameter (while keeping transverse pitch constant) can result in increased velocities, turbulence, and Reynolds number.

The recirculation zones behind each tube have tiny overflow areas in the case of greater air flow. The second recirculation zone looks to be greater than the first. A recirculation zone was not visible in the instance with a 0.3 m/s inlet velocity, as it was in the case with a 6.2 m/s inlet velocity.

*D. Comparison of Numerical and Experimental Results*

For ten inflow velocities, data on pressure drop, maximum velocity, and heat transfer coefficient are recorded. Friction factor and Coburn j-factor are derived using these recorded values. To compare with experimental data, the Fanning friction factor f is listed in Table 5.3 and plotted against Reynolds number in Figure 5.7. The graph (Figure 5.7) shows that simulated and experimental values follow the same trend. Figure 5.8 depicts the % error in simulated values compared to experimental friction factor f values.

| Re | Fanning friction factor f (Numerical Results) | | |
|---|---|---|---|
| | Laminar | k-epsilon | SST k-omega |
| 330 | 0.114301 | 0.12834 | 0.11573 |
| 600 | 0.078958 | 0.085486 | 0.08113 |
| 790 | 0.063243 | 0.066578 | 0.066373 |
| 1300 | 0.049123 | 0.048782 | 0.053733 |
| 1700 | 0.042439 | 0.040209 | 0.046074 |
| 2900 | 0.033973 | 0.030271 | 0.034262 |
| 4300 | 0.028998 | 0.02524 | 0.028268 |
| 5200 | 0.027105 | 0.023353 | 0.02569 |
| 6200 | 0.025445 | 0.022123 | 0.02361 |
| 7200 | 0.024416 | 0.021219 | 0.022234 |

Table 5.3: Fanning friction factor f (Numerical Results)

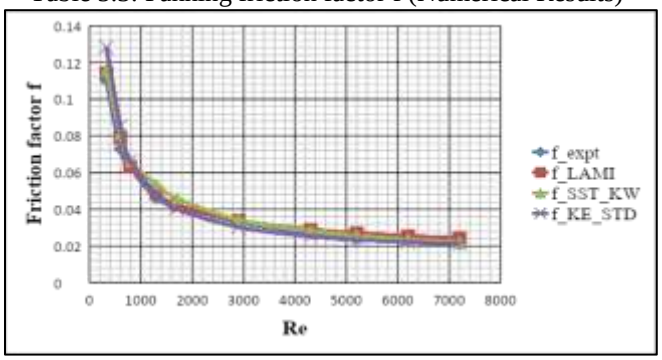


Comparison of experimental and numerical values for friction factor f

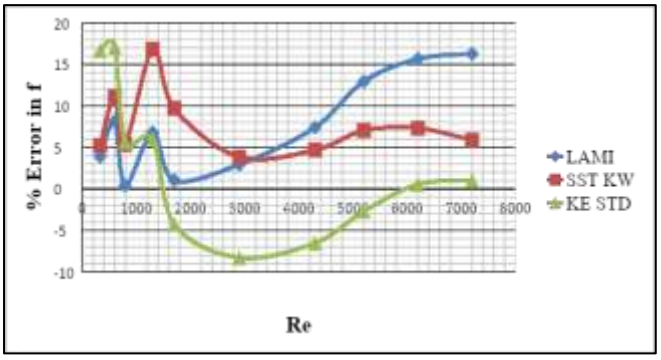


Percentage error in friction factor f

The Coburn j-factor is tabulated and compared to the experimental value in the same way. Finally, the % error for simulated values against experimental values is presented.

| Re | Colburn j factor (Numerical Result) | | |
|---|---|---|---|
| | Laminar | k-epsilon | SST k-omega |
| 330 | 0.034964 | 0.039524 | 0.035225 |
| 600 | 0.027451 | 0.032419 | 0.027989 |
| 790 | 0.023432 | 0.027021 | 0.02414 |
| 1300 | 0.018764 | 0.021256 | 0.020222 |
| 1700 | 0.015851 | 0.017826 | 0.017801 |
| 2900 | 0.01165 | 0.012691 | 0.013595 |
| 4300 | 0.00879 | 0.009822 | 0.010913 |
| 5200 | 0.00784 | 0.008457 | 0.009719 |
| 6200 | 0.006792 | 0.007277 | 0.008869 |
| 7200 | 0.00596 | 0.006512 | 0.007978 |

Colburn j-factor (Numerical Results)

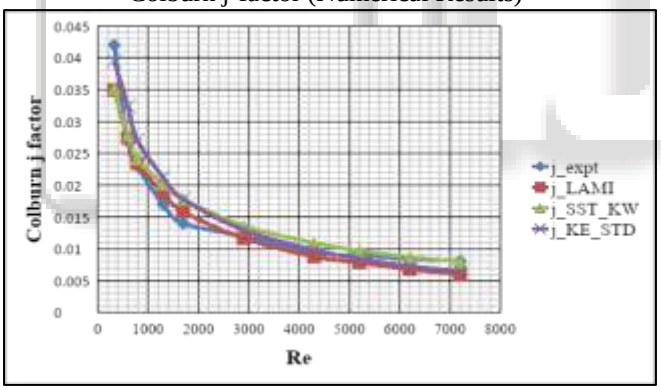


Comparison of experimental and numerical values for Colburn j-factor

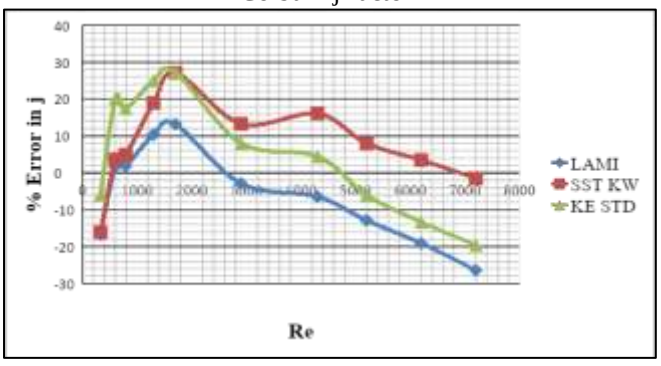


Percentage error in Colburn j-factor

The simulation results for the different flow models were used to calculate the heat transfer characterization parameter Colburn j-factor. At different Reynolds numbers, the flow models reveal extremely clear differences in their ability to replicate heat transfer. The laminar flow model, as expected, is the best for forecasting the j-factor in laminar flow. A laminar and k-epsilon turbulence model is excellent for describing transition heat flow, whereas the k-omega model is best for calculating turbulent heat flow.

## VI. Conclusion and Future Scope

### *A. Conclusion*

The objective of this project is to develop the CFD simulation model for two-row fin-and-tube heat exchanger and verify the results of simulation with the available experimental data from the literature. The purpose of the work was to investigate the possibilities of eventually using CFD calculations for design of heat exchangers instead of expensive experimental testing and prototype production.

To analyse the flow and heat transfer characteristics of the heat exchanger, a model of a two-row fin-and-tube heat exchanger is created using Design modeller and Mesh module to create the geometry and mesh respectively. The resulting mesh (after a grid independence test was carried out) is used for running simulations using a laminar flow model and two turbulence models. Ten different inlet flow velocities ranging from 0.3 m/s to 6.2 m/s and corresponding to Reynolds numbers ranging from 330 to 7200 are simulated in the three different flow models (laminar, k-epsilon turbulence model, and SST k-omega turbulence model). Using the simulation results calculations related to heat flow and pressure loss are carried out to determine the Fanning friction factor f and Colburn j-factor for comparison with the literature values used for the validation.

It is found that the flow model accuracy depended on the flow regime and whether the friction factor f or j-factor is being determined. From the experimental values given in the literature, the laminar flow region for this particular geometry of heat exchanger switched to transitional at around Reynolds number 1300, and moving to turbulent around Reynolds number 2900. The Reynolds number has a characteristic dimension of the tube collar outside diameter.

The flow model can be chosen based on what is being studied (heat flow or pressure drop) and the flow regime. It can be concluded that the pressure drop and heat transfer characteristics of a fin-and-tube heat exchanger can be determined with reasonable accuracy using CFD computations carried out in ANSYS Workbench. These results can be used to carry out practical work in the design process of heat exchangers.

### *B. Future Scope*

In the present study, the thickness of the wing vortex generator is not considered. A more accurate model would be to consider the finite thickness of the parallel plates of the plate-fin channel and of the wings vortex generator. It would be a conjugate heat transfer problem and the solution will yield more exact predictions. The computations have been done assuming the flow regime to be laminar. Although turbulent flow is not frequently encountered in plate-fin heat exchangers, in some special applications involving very high velocities, the flow regime can become turbulent. Therefore, the present study can be extended by considering turbulent flows. Using an appropriate turbulence model, the

 

performance of the proposed design can be computed for higher Reynolds numbers.

## REFERENCES

[1] Yuzhu Zhou, Lin Zhang, Shi Bu, Cheng Sun, Weigang Xu, Yongchang Xiao and Lin Liu, [Study on Heat Transfer Characteristics of the Whole Plate Fin Tube Cooler], International Journal of Thermofluid Science and Technology (2020) Volume 7, Issue 2, Paper No. 070204.

[2] Subodh Bahirat and P. V. Joshi, [CFD Analysis of Plate Fin Tube Heat Exchanger for Various Fin Inclinations], Subodh Bahirat Int. Journal of Engineering Research and Applications, ISSN : 2248-9622, Vol. 4, Issue 8( Version 3), August 2014, pp.116-125.

[3] M. Shawky Ismail, M. Hassab and Wael M. El-Maghlany, [Comparative Three Dimensional CFD Study for Inline Cross Flow Plate Finned Tube Heat Exchanger], Proceedings of the 4 th World Congress on Momentum, Heat and Mass Transfer (MHMT'19) Rome, Italy – April, 2019.

[4] Ishwar J.Dhangar and Dr. Manojkumar Chopra, [Experimental Investigation and CFD Analysis Performance of Fin and Tube Heat Exchanger with Different Types of Fins], International Journal of Engineering Research & Technology (IJERT) ISSN: 2278-0181. Special Issue - 2017.

[5] K. Ranjithkumar, M. Santhoshkumar and R. Periyasamy, [Experimental and Numerical Analysis of Heat Transfer on Plate Fin Heat Exchanger at Different Fin Pitches with Ceramic Coating], International Journal of Engineering Research & Technology (IJERT) ISSN: 2278-0181 Published by, www.ijert.org ICITMSEE - 2018 Conference Proceedings.

[6] Mladen Bošnjakovi´c and and Simon Muhi˘c, [Numerical Analysis of Tube Heat Exchanger with Perforated Star-Shaped Fins], Fluids 2020, 5, 242.

[7] Yuvraj Singh Rajput and Abhishek Arya, [CFD Analysis of Cross Flow Heat Exchanger with Different Fin Thickness], INTERNATIONAL JOURNAL OF INNOVATIVE RESEARCH IN TECHNOLOGY, July 2019 | IJIRT | Volume 6 Issue 2 | ISSN: 2349-6002.

[8] Abhishek Mishra and Dr. Nitin Tenguria, [Experimental Investigation of Heat Transfer in Modified Finned Tube Banks Arrangement with in-Line and Staggered Layout], INTERNATIONAL JOURNAL OF INNOVATIVE RESEARCH IN TECHNOLOGY, August 2020| IJIRT | Volume 7 Issue 3 | ISSN: 2349-6002.

[9] Arafat Ahmed Bhuiyan and A K M Sadrul Islam, [CFD analysis of different Fin-and-Tube Heat Exchangers], Proceedings of the 13th Annual Paper Meet 25 September 2010, Dhaka.

[10] Young-Chang Liu, Somchai Wongwises, Wen-Jeng Chang and Chi-Chuan Wang, [Airside performance of fin-and-tube heat exchangers in dehumidifying conditions – Data with larger diameter], International Journal of Heat and Mass Transfer 53 (2010) 1603–1608.

[11] Wenxiao Chu, Pengqing Yu, Ting Ma, Min Zeng and Qiuwang Wang, [Numerical Analysis of Plain Fin-and-Oval-Tube Heat Exchanger with Different Inlet Angles], Chemical Engineering Transactions, VOL. 35, 2013.

[12] Shubham Gupta and Karan Singh Verma, [COMPUTATIONAL FLUID DYNAMICS ANALYSIS OF SHELL AND TUBE HEAT EXCHANGER WITH HAVING DIFFERENT TYPES OF FINS], International Journal for Research Trends and Innovation, 2022 IJRTI | Volume 7, Issue 2 | ISSN: 2456-3315.

[13] Artur Rubcov, Sabina Paulauskaitė and Violeta Misevičiūtė, [Experimental Analysis of Fin and Tube Heat Exchanger in Heating and Cooling Mode], "Environmental Engineering" 10th International Conference, Lithuania, 27–28 April 2017.

[14] Xuehong Wu, Lihua Feng, Dandan Liu, Hao Meng, and Yanli Lu, [Numerical Study on the Effect of Tube Rows on the Heat Transfer Characteristic of Dimpled Fin], Hindawi Publishing Corporation Advances in Mechanical Engineering Volume 2014, Article ID 637052, 9 pages.

[15] Zena K. Kadhim, Muna S. Kassim and Adel Y. Abdul Hassan, [CFD study for cross flow heat exchanger with integral finned tube], International Journal of Scientific and Research Publications, Volume 6, Issue 6, June 2016, ISSN 2250-3153.

[16] Ahmed F. Khudheyer and Mahmoud Sh. Mahmoud, [NUMERICAL ANALYSIS OF FIN-TUBE PLATE HEAT EXCHANGER BY USING CFD TECHNIQUE], ARPN Journal of Engineering and Applied Sciences, VOL. 6, NO. 7, JULY 2011.

[17] Animesh Kumar, Divyansh Singh, Aman Deep Singh, Mayank Chauhan, Keshav Nath Chaturvedi and Amit Singh, [Optimization of Fin and Tube Heat Exchanger], International Journal of Innovative Science and Research Technology ISSN No:-2456-2165, Volume 3, Issue 5, May – 2018.

[18] A.Y. Adam, A. N. Oumer, Azri Alias, M. Ishak, R. Mamat, and A. Abdul Adam, [Thermal and Fluid Dynamic Analysis of Compact Fin-and-Tube Heat Exchangers for Automotive Applications], MATEC Web of Conferences 225, 05019 (2018).

 